IEEE Access
Multidisciplinary | Rapid Review | Open Access Journal

Received October 21, 2019, accepted November 8, 2019, date of current version November 21, 2019.

Digital Object Identifier 10.1109/ACCESS.2019.2953259

An Improved Retinal Vessel Segmentation Framework Using Frangi Filter Coupled With the Probabilistic Patch Based Denoiser

AHSAN KHAWAJA, TARIQ M. KHAN, (Member, IEEE), KHURAM NAVEED, SYED SAUD NAQVI, NAVEED UR REHMAN, AND SYED JUNAID NAWAZ, (Senior Member, IEEE)

Department of Electrical and Computer Engineering, COMSATS University Islamabad (CUI), Islamabad 45550, Pakistan

Corresponding author: Ahsan Khawaja (ahsan_khawaja@comsats.edu.pk)

This work was support in part by the Project MEDiCS under Grant ICI-RDO-MoE-KSA-2018.

ABSTRACT Vessel segmentation has come a long way in terms of matching the experts at detection accuracy, yet there is potential for further improvement. In this regard, the accurate detection of vessels is generally more challenging due to the high variations in vessel contrast, width, and the observed noise level. Most vessel segmentation strategies utilize contrast enhancement as a preprocessing step, which has an inherent tendency to aggravate the noise and therefore, impede accurate vessel detection. To alleviate this problem, we propose to use the state-of-the-art Probabilistic Patch-Based (PPB) denoiser within the framework of an unsupervised retinal vessel segmentation strategy based on the Frangi filter. The PPB denoiser helps preserve vascular structure while effectively dealing with the amplified noise. Also, the modified Frangi filter is evaluated separately for tiny and large vessels, followed by individual segmentation and linear recombination of the binarized outputs. This way, the performance of the modified Frangi filter is significantly enhanced. The performance evaluation of the proposed method is evaluated on two recognized open-access datasets, viz: DRIVE and STARE. The proposed strategy yields competitive results for both preprocessing modalities, i.e., Contrast Limited Adaptive Histogram Equalization (CLAHE) and Generalized Linear Model (GLM). The performance observed for CLAHE over DRIVE and STARE datasets is ($Sn = 0.8027$, $Acc = 0.9561$) and ($Sn = 0.798$, $Acc = 0.9561$), respectively. For GLM, it is observed to be ($Sn = 0.7907$, $Acc = 0.9603$) and ($Sn = 0.7860$, $Acc = 0.9583$) over DRIVE and STARE datasets, respectively. Furthermore, based on the conducted comparative study, it is established that the proposed method outperforms various notable vessel segmentation methods available in the existing literature.

INDEX TERMS Image denoising, image segmentation, modified Frangi filter, probabilistic patch-based denoiser, retinal vessels.

I. INTRODUCTION

Vascular segmentation is vital for examining pathologies inside and around the retinal periphery. These vessels help differentiate between retinas that are healthy with those suffering from various ocular pathologies such as occlusions, Diabetic RetinoPathy (DRP), etc. An Ophthalmologist would have to manually label the vessels of the retina, which is both time and labor exhaustive. This method is also prone to human error, emphasizing the need for an automated computer system capable of segmenting the vessels within acceptable ranges of accuracy [1]. A computer-aided diagnostic system can be crucial in determining various ocular pathologies with accuracy and consistency. Such a setup will lead to ever more capable health care tools in the hands of medical experts, where it will serve a dual purpose of better resource management and automated tracking of disease progression.

For this purpose, vessels within a retinal fundus image are labeled using a binary classification process whereby all the pixels are classified as either a vessel or non-vessel pixel. This challenging task has attracted considerable research interest over the years, leading to the development of both supervised and unsupervised learning methods. The supervised

The associate editor coordinating the review of this manuscript and approving it for publication was Omar Sultan Al-Kadi.

methods require a training regimen for which the ground truth feedback is highly important and may or may not be readily accessible. Unsupervised methods, on the other hand, operate independently of human assistance or prior training, and thus come with their own set of pros and cons. Automatic vessel detection has reached considerably high accuracy rates, yet invariably all methods suffer at detecting tiny vessels in more challenging images with varying sensitivity rates [2]. Complicated vessel geometry and retinal pathologies such as glaucoma, hypertension, DRP, and Age-related Macular Degeneration (AMD) further degrade the performance of the vessel segmentation techniques [3], [4].

Electronic fluctuations and scattering phenomena during the fundus imaging process introduce noise within the acquired image. In this regard, the additive noise is caused by the system's electronic components, whereas the scattering phenomena in laser imaging cause speckle patterns in the acquired image. These patterns of speckle are characterized by a multiplicative noise model and cause considerable deterioration of the captured blood vessels, especially the smaller ones. As a consequence, the process of noise removal is not alien to the computerized detection of retinal features in fundus image processing. However, the use of basic noise removal methods, e.g., Weiner filter, limit their practical use because of the significant loss of image details (i.e., vessel endpoints).

This problem of noise is further aggravated by the preprocessing operations, aiming to extract vessels out of poor contrast regions in a fundus image. Considerable enhancement in the contrast of the fundus image is crucial for the effective classification of the vessel and non-vessel pixels. This, in turn, results in the noise getting inflated, thereby affecting the efficacy of the subsequent segmentation stages. Therefore, a substantial improvement in contrast, as well as noise suppression, is required before segmentation. An image contrast normalization step paired with a capable denoiser would help meet the goal of a high sensitivity measure after segmentation.

Retinal fundus images suffer from both the additive and multiplicative noise. The additive noise is modeled using the Additive White Gaussian Noise (AWGN), and the multiplicative noise is modeled as Rayleigh distributed speckle noise [5]. These noise artifacts obscure tiny vessels, particularly in low contrast regions [6] that prevent the efficient detection and segmentation of these small vessels. Owing to the significance of the problem, researchers have developed denoising methods exclusively for retinal fundus images [6]–[8]. These methods strive to tackle the complexity of simultaneously dealing with both additive and multiplicative noises by cascading both noise models into the denoiser [3]. However, these methods have limited applicability because of the loss of too many details through the use of such complicated denoisers.

Owing to the fundamental nature of the problem of noise removal, image denoising is a well-studied domain. Researchers have come up with a wide variety of methods [9]–[14] which effectively suppress noise without losing image singularities. These state of the art methods yield the highest level of image quality because of the precise noise and signal models used within these methods. In this regard, denoising methods specifically employed to reduce systematic additive noise, generally use the AWGN model while those designed to tackle speckle noise use the Rayleigh distribution model. Naturally, the use of these evolved denoising strategies would be vital in dealing with the noise in fundus images, whereby the reduction of speckle patterns is crucial to the detection of small vessels.

This paper suggests the use of a state of the art denoiser alongside an unsupervised learning strategy based on the modified Frangi filter to improve upon the detection of vessels. The suggested pipelined framework first employs the Singular Value Decomposition (SVD) for robust contrast enhancement, followed by equalization through both Contrast Limited Adaptive Histogram Equalization (CLAHE) and Generalized Linear Model (GLM). Subsequently, the denoiser takes care of the noise which was further amplified by the SVD. For that purpose, we propose the use of the Probabilistic Patch-Based (PPB) speckle denoiser [11] to fundus images because it ensures the maximum retention of blood vessels, including the inconspicuous smaller vessels owing to its complex multi-step procedure.

We classify the vessels into two categories as: large vessels (with diameters larger than 3 pixels), and small/tiny vessels (all others). For the purpose of tiny vessel detection, modified Frangi method (an improved version of the an earlier Frangi filter) with a larger Gaussian scale is employed as it is based on an analytic model for the elongated tubular structures. The vessels with larger width are captured using a smaller Gaussian scale of the modified Frangi method. Towards the end of large and small-width vessel detection, binary conversion takes place separately, and the output is linearly combined. The main contributions are:

- Use of enhancement factor in the modified Frangi to improve its performance.
- Dividing vessels into two categories and segmenting large and tiny vessels separately with modified Frangi.
- Denoising large vessels with PPB speckle denoiser.

This research paper is organized into five sections, where sections II and III discuss the related work and the proposed method in detail, respectively. Section IV comprises of the tested repositories and parameters employed to evaluate the efficiency of this technique. The results of the experiment and its comparison with other detection techniques are also elaborated in this section, ending with section V summarizing the conclusions of this study in terms of the efficacy, pros, and cons of the method.

II. RELATED WORK

The analysis of the retinal vessel tree has enjoyed tremendous focus over the past decade. Researchers have employed a

wide array of image processing techniques to achieve this segmentation task, e.g., Pattern Recognition (PR), vascular tree tracing, model-based (region/edge), etc. PR methods can further be summarized into two broad classes of either supervised (guided) versus unsupervised (self-learning) segmentation methods. What follows, is a review of the best performing techniques put forth over the past decades belonging to either of these two categories.

A. SUPERVISED LEARNING METHODS

These depend upon predefined statistical or morphological markers from gold standard (expert marked) images to differentiate between the vessel and non-vessel pixels. Supervised methods evolve the relevant feature markers extracted from either the local or global data, by training a Neural Network (NN) or by following an ensemble-based approach using these expert-marked images. Hence, the availability of gold standard images is key for supervised methods, and the lack of availability of such images poses a big problem. It is also noteworthy that there is a great deal of discourse even among the experts on the matter of marking the retinal vessels [15].

Supervised techniques generally outperform their unsupervised competitors solely because they draw their strength from pre-defined data for training the classifier [16]. K-Nearest Neighbor (KNN) classifier was employed by both Staal *et al.* [17] (to identify ridge features) and Niemeijer *et al.* [18] (Gaussian derivatives) during the vascular segmentation process. Soares [19] used Gabor filter (based on wavelets obtained at multiple scales), and Gaussian Mixture Model (GMM) classifier for supervised vessel detection. Roychowdhury *et al.* [20] presented a three-layered approach where binarized masks from both the green channel image and a morphological base image are used to extract the major vessels. The remaining pixels are classified utilizing a GMM to carve out the finer pixels, which are eventually coupled with the major vessels to evolve the overall retinal vasculature.

As the experiment's parameters are tuned for better detection results, this has a substantial impact on unsupervised methods as compared to the more immune supervised techniques. Still, all the methods discussed above suggest better vessel detection outcomes whenever a similar hybrid learning approach is deployed. Ricci and Perfetti exhibited the same with line operators trained by a Support Vector Machine (SVM), thereby displaying reasonably good results with both normal and noisy images. Another more sophisticated technique involves training NN for solving classification problems such as the one used by Marin *et al.* [22]. He used gray-level based features that were consistent with varying moments. This enabled the setup to be trained on arbitrary image settings and databases. Other works such as [23] and [24] demonstrated the usefulness of a NN, where the pixel classification depends more on statistical probabilities instead of objective reasoning.

B. UNSUPERVISED LEARNING METHODS

These methods exploit the intrinsic characteristics of an image to look for recurrent features that help differentiate between the foreground and the background. Such techniques thus do not depend upon the expert marked images, and work independently of any guidance from the ground truth images or training data. In the absence of any manual annotations, vessel segmentation is achieved by making use of image processing techniques such as multiple scale-based methods, matched filtering approaches, mathematical/morphological techniques, and region-growing methods.

Multi-scale methods make use of scale-space, where the variations in input image scales are used to segment out various structures. This attribute finds particular use in vessel segmentation, as vessels in retina come in vastly varying orientations and sizes. Main vessel branches are extracted from the low contrast image, and high contrast versions are employed for the extraction of tiniest vessels usually located at the endpoints of the vessel tree. Frangi *et al.* [25] coupled Hessian vessel width estimator with noise and background suppression for vessel extraction. The low visibility vessels were successfully detected right down to branching angle measurements, with considerable False-Positive Rate (FPR) reduction as well as salt and pepper noise immunity. Azzopardi and Petkov [26] used a Combination Of Shifted FIlter REsponses (COSFIRE) function that emphasized circular geometric attributes for the detection of vessels around a focused spatial periphery. This method exhibited high performance parameters in healthy images but suffered a high FPR in pathological images.

An innovative retinal vasculature extraction technique based on a QUARTZ [27] algorithm by Fraz et al., employed a vascular diameter calculation and curvity measure to trace out the retinal vessels from the Optic Disc (OD). A percentile-based threshold is stated by Annunziata *et al.* [28], which is coupled with the multi-scale Hessian eigenvalues method to significantly diminish the FPR, especially in pathological images. This method excels in images with abnormalities such as exudates, where a neighborhood estimator with a gap filling function helps the detection of vessels in and around these exudates. Emary *et al.* [29] reported a novel flower pollination search algorithm geared towards the detection of the smaller vessels via Fuzzy C-Means (FCM) clustering. This setup excelled in vessel detection reporting a sensitivity of 0.9378 and specificity of 0.8994.

Mathematical Morphological (MM) processes involve probing a selected portion of the retinal image with a little scanning element referred to as a kernel. This kernel iterates upon all possible locations within the image, infusing them with excellent immunity against linear and nonlinear noise by taking influence from nearby pixels. Mendonca and Campilho [30] presented a pixel processing based Difference of Set Gaussian (DoSG) function that relied predominantly on detecting the vessel centerline. Enhancement via line detector function at varying angles helped the morphological

reconstruction of varying vessel widths through an iterative region growing routine.

Fraz *et al.* [31] introduced bit-plane slicing (based on morphology) coupled with vessel mid-line identification to successfully extract the retinal vasculature. The differential filtering induced noise tolerance to the algorithm in both normal and pathological images. Sigurdhsson *et al.* [32] proposed an efficient vessel pixel categorization system based on path opening filters that efficiently segmented major and minor vessels with relative noise robustness. The algorithm is overseen by data fusion operators, followed by fuzzy set theory to recreate retinal vessel tree. Imani *et al.* [33] extracted noise-immune retinal vessel attributes through Morphological Component Analysis (MCA). A wavelet transform proceeded by an adaptive thresholding regimen is used to bifurcate lesion and vessel pixels with a high degree of accuracy.

Matched Filtering (MF) techniques contrast a sample sub-image segment against pre-established filter responses to label those samples as vessel versus non-vessel pixels. Vessel isolation is achieved from a 2-D template that probes for a local matching response against the known optical entity responses, such as a vessel at multiple orientations. To make the template effective, the following vessel attributes are taken into consideration: vessel structural elongation, branch, crossover points, and the inter-vessel size differences. Apart from computational complexity, any template or kernel responds preferably to vessels only when the vessel profile matches the filtered profile of that kernel. A pathological image proves to be a challenge where indistinguishable neighborhood elements cause a spike in false detections. MF techniques are mostly found effective when used in conjunction with other detection methods.

Chaudhuri *et al.* [34] segregated retinal vessel tree by using a feature recognition operator, relying upon the optical and spatial traits of a vessel. The cross-sectional area of a vessel is estimated using a preset number of ingenious rotating Gaussian profiles. Twelve assorted kernels, each turning 15 degrees map the vascular terrain correctly, classifying between vessel and non-vessel pixels. Hoover *et al.* [15] structured a procedure for the vessel identification employing neighborhood and area-based characteristics of the retinal vessel tree, followed by iterative threshold testing. Afterwards, the process is repeated by the inclusion of non-vessels pixels into the test pool. This methodology accomplished significant gains, both in the output true-positive and false-positive rates, as more rigorous testing of non-vessel pixels proved to be crucial. Al-Rawi *et al.* [35] modified the methodology in [34] by making use of a complete search enhancement procedure based on statistical threshold limits. Tests on the DRIVE images resulted in a high accuracy score as optimal characteristics were gauged under size-based and standard deviation kernels.

Region Growing (RG) techniques are based on vessel isolation, utilizing comparable pixel traits around a close vicinity. The effectiveness of such methods depends upon the selection of the initial seed point and expansion rules. As the vessels occur over a broad range of gray-levels, a traditional manual input of the seed point makes it difficult to accurately map the vessel structure. If similar thresholds are applied to the entire seed point population, the rate of region growth can easily be controlled right up to the narrowest of vessels. Ahmad Fadzil *et al.* [36] developed an iterative region developing methodology utilizing various statistical and morphological pointers to segment out the vessels. Methods such as contrast limited adaptive histogram equalization (CLAHE) coupled with contrast stretching alongside bottom-hat filter (opposite of a top-hat filter), and a mean filter are employed to extract the vessel feature markers. RG methods, using either the seeds or gradients for vascular recreation, help such methods achieve high performance metrics in both sensitivity and specificity.

Zhao *et al.* [37] presented a method that relied on improving the vessel segregation by means of CLAHE and 2-D Gabor filter. Vessel extraction is preceded by illumination equalization to retain the finer edges of small vessels. Enhanced images are then subjected to RG based on a level set function to distinguish between vessel and non-vessel pixels. Dizdaroğlu *et al.* [38] proposed a progressive zero-level isometric profile normalization, resulting in high accuracy and specificity measures. This is more appropriate than other similar methods, where a structure-oriented region growing method is used alongside an automated seed point generation. This setup was tested on publicly available datasets along with the authors own data set and exhibited equally effective vessel segmentation for both healthy and pathological retinal images.

Zhang *et al.* [39] defined an autonomous retinal segmentation method using Gaussian derivatives to maintain vascular orientation ratings, which are later used as the fitness function for the algorithm. Elongated vessel structures are enhanced throughout the image, resulting in much improved tiny vessel segmentation. Vessel identification strategies based on multiple scales, sizes, and orientations help this method score high in both accuracy and sensitivity parameters. A programmed seed point selection relying on binary symmetry decision for each pixel, is presented by Panda *et al.* [40]. The algorithm hunts for vessel mid-line pixels by means of a novel Binary Hausdorf Symmetry (BHS) measure followed by seed placement based on the pixel edge distance from the vessel mid-line. This method reports the highest vessel detection accuracy among all RG methods, yet this technique's main hindrance is its strong reliance on the state of vessel edges.

Some recent methods such as Soomro *et al.* [41], use Principle Component Analysis (PCA) prior to gray-scale conversion to achieve a considerable improvement in sensitivity. Varying scales of these components were employed for normalization, followed by anisotropic diffusion to specifically target narrow vessels. Khan *et al.* [42] used blob detection for circular and elliptical shaped objects, based on a set of necessary conditions adopted for real images. A multi-scale framework of a Generalized Laplacian of Gaussian (GLOG)

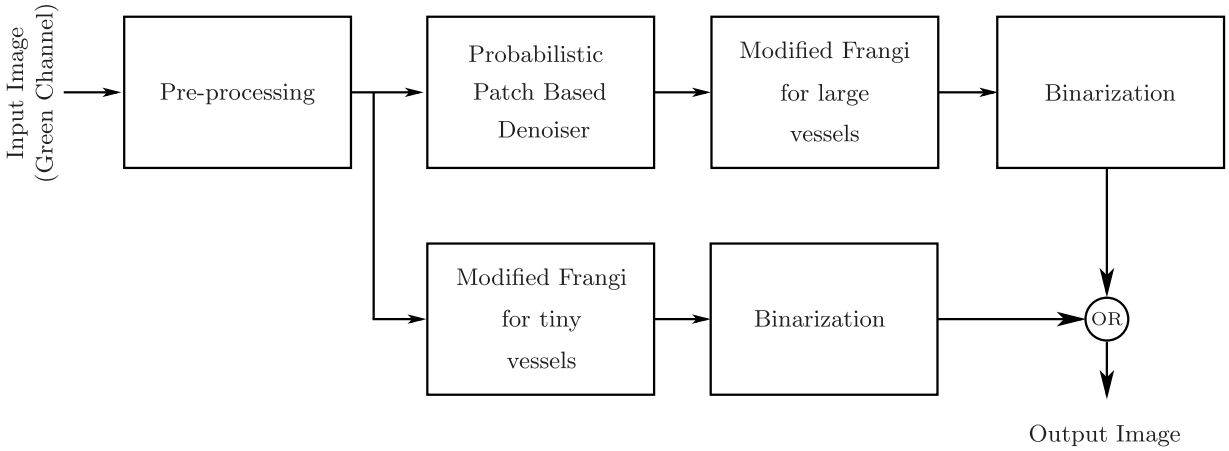

FIGURE 1. Proposed methodology.

detector is validated by synthetic and real world image sets. Khan *et al.* [43] used the multi-scale line detectors aided by externally fed orientations to align the detector. Sensitivity in contrast was tackled by a hysteresis threshold as more and more orientations fields are explored.

Soomro *et al.* [44] employed Independent Component Analysis (ICA), where images were treated as random variables and their pixels as the traits for contrast enhancement. These traits exhibit a high co-relation probability as two models ICA1 and ICA2 were simultaneously used to enhance finer vessels and suppress noise, respectively. Khan *et al.* [45] and Shahid and Taj [46] used noise removal and Frangi filter, followed by raster to vector conversion using the Vessel Location Map (VLM). These methods reported high detection accuracy along with faster computation times. Chalakkal and Abdulla [47] used the Fast Discrete Curvelet Transform (FDCT) coupled with a modified line detector on DRIVE dataset to achieve specificity and accuracy of 0.9542 and 0.9735, respectively.

Both the supervised and unsupervised vessel segmentation methods have seen researchers come up with ingenious ways to deal with problems such as:

- Uneven illumination during image acquisition.
- Complexity of vascular structures.
- Retinal pathologies.
- Trade-offs between performance parameters such as sensitivity versus accuracy.
- Limited and unbalanced datasets.

Frangi filter has been the method of choice for numerous vessel segmentation techniques due to its inherent ability to hunt for tubular entities within a frame of reference. The big advantage of this filter is its flexibility towards larger images, as it incorporates a multi-scale instead of a fixed-scale approach. However, the main limitations of detectors such as Frangi filter and line detectors, come in the form of image noise, branching nodes, and vessel crossings which confuse the segmentation algorithm into generating a higher number of false-positives [43], [44], [48]. Another drawback of Frangi filter is the misclassification of pixels near the boundary of a vessel, where non-uniform illumination causes the filter to become weak.

III. PROPOSED METHOD

The primary objective of this study is efficient vessel segmentation, through improvement in the quality of the input retinal image by enhancing contrast while keeping the noise artifacts at bay. The overall methodology can be summarized as:

1) Contrast enhancement of the retinal image utilizing SVD.
2) Employing CLAHE and GLM on the green channel of the RGB image.
3) Using the PPB denoiser to mitigate the effects of noise amplification in contrast enhancement phase.
4) Using the modified Frangi method to segment the large and small vessels separately for improved vascular segmentation.

Fig. 1 illustrates the overall flow chart of the proposed technique.

A. COLOR IMAGE CONTRAST NORMALIZATION THROUGH SINGULAR VALUE DECOMPOSITION (SVD)

Generally, the inherent contrast of an image is unsuitable for applying more sophisticated image processing techniques. Especially, the low contrast of the input image affects the color to gray-scale transformation. This problem domain has attracted a lot of research interest, as contrast enhancement leads to more efficient post-processing when compared with the original image. Global Histogram Equalization (GHE) is a powerful technique used to stretch the contrast band to fully utilize the available dynamic contrast range.

Local Histogram Equalization (LHE) is another similar technique that operates on a narrower contrast band, resulting in more target-oriented contrast adjustment. Both these methods are found lacking in the sense that during the equalization process, the adjustment seldom exceeds the desired enhancement levels, resulting in the addition of artifacts to

the original image. This, in turn, deprives the image of its original look and feel, causing other intermittent problems in the sophisticated post-processing methods the image must further go through.

GHE, LHE, and other similar contrast adaptation methods suffer from lack of scalability in the applied enhancement. SVD is one such contrast adjustment method, with the added versatility that it can be employed in both the frequency and pixel domains. The SVD method overcomes this problem by providing a degree of control over the desired level of contrast enhancement that can be tuned to the nature of the image. This flexibility in contrast enhancement, makes this technique a widely featured in image segmentation, compression, and object recognition. Improving the contrast of low contrast images is another strong avenue for SVD where the illumination aspect is targeted in particular. For this study, SVD was employed for contrast improvement. In this method, a singular vector matrix is obtained through the equalization of SVD.

A matrix representing the SVD of an image, is described as:

$$A_{(SVD)} = U_X \sum\nolimits_X V_X^T, \tag{1}$$

where U_X is an orthogonal square matrix termed as the hanger. V_X is another similar matrix termed as the aligner. The $\sum_X$ matrix has all the singular terms placed along its diagonal, which describes the overall intensity information of the image. Any change in these singular terms alters the intensity profile of the image, thus helping in the equalization process. The input image undergoes RGB to HSV conversion, following which the V channel has SVD applied on it. The resultant matrix is then acted upon by SVD (with mean equal to zero and unit variance), yielding the desired singular terms as depicted below:

$$\xi = \frac{\max\left(\sum_{N(\mu=0,var=1)}\right)}{\max\left(\sum_X\right)}, \tag{2}$$

where $\sum_{N(\mu=0,var=1)}$ represents the matrix having artificial intensity singular values. The final image, after all these equalization steps is regenerated by the expression:

$$A_{Eql} = U_X \left(\xi \sum\nolimits_X\right) V_X^T. \tag{3}$$

Output of these steps is presented in Fig. 2.

FIGURE 2. SVD color contrast enhancement.

B. NON-UNIFORM ILLUMINATION REMOVAL

The details of non-uniform illumination removal are presented in this section.

1) CONTRAST LIMITED ADAPTIVE HISTOGRAM EQUALIZATION (CLAHE)

Improving the image contrast is a vital preprocessing step that is widely employed in pattern recognition, medical imaging, and computer vision. The crux of image enhancement lies in the fact that, the texture and overall appearance of the image have to be preserved without any over or under-enhancement alongside noise suppression. Weak image sensors, uneven exposure, and poor ambient light are few among the many contributing factors towards an image having distorted contrast and poor dynamic range.

CLAHE is an improved type of Adaptive Histogram Equalization (AHE) developed by Zuiderveld [49] to enhance low contrast bio-medical images. The primary drawback in AHE, is the proportional enhancement in both contrast and noise, especially in uniform gray-level regions. CLAHE alleviates the noise amplification problem by dividing an image into small inter-related areas called tiles, followed by applying histogram equalization over each tile. CLAHE has been the method of choice for many researchers during the preprocessing phase, as it yields more pronounced hidden features and edges. This is achieved by improving the local contrast, thereby making full use of the available gray-level spectrum. For our experiment, values for the number of tiles (8 by 8), and contrast enhancement clip limit (0.01) were empirically gauged as optimum.

2) GENERALIZED LINEAR MODEL (GLM)

The main goal of any preprocessing procedure prior to segmentation, is to make the foreground (region of interest or vessels in our case) more prominent as compared to the background. Hence, to make the detector's job easier, morphological operators having circular structuring elements are used to remove non-vascular features. This is done by means of an adapted top-hat transform that employs special opening and closing operators. The opening operator preserves the pixel values, apart from the regions that are smaller than the structuring element and have a higher intensity. The closing operator on the other hand, replaces any detail that is smaller than the structuring element with higher nearby intensities. In simpler words, the opening operation tends to remove the vessels whereas, the closing operation tends to minimize background fluctuations.

The opening and closing top-hat transformations on the green channel image (I_G), are done with the structuring elements S_{close} and S_{close}, respectively. These operators are further elaborated as:

$$T_{\text{open}} = I_G \circ S_{\text{open}}, \tag{4}$$

$$T_{\text{close}} = I_G \bullet S_{\text{close}}, \tag{5}$$

where ($\circ$) and ($\bullet$) represent the opening and closing top-hat operators, respectively. An enhanced adaptation of top-hat transform, as suggested in [50], is given by:

$$T_E = I_G - (I_G \bullet S_{\text{close}}) \circ S_{\text{open}}. \tag{6}$$

Disk-oriented structuring elements with a radius of 8 pixels were used in both these operators. Using this morphological operator, exclusive contrast enhancement for vascular entities is achieved by first removing other retinal features such as OD, macula, and any other pathologies. This is followed by the acquisition of a feature set through a single pass of GLM regression over the ground truth image, thereby helping to boost the vessels and suppress background pixels.

To understand GLM, it is useful to discuss a common type of predictive analysis known as simple linear regression. It is a scalar response that aims to find a linear relationship (fitting a linear equation) between a normally distributed dependent variable and an independent variable. When this association is made to more than one independent variables, it becomes a multiple linear regression. In cases where the outcomes are not normally-distributed, a general model is needed which is capable of adapting to other forms of distributions. GLM is thus, a technique that tries to generalize linear regression. This is done by doing linear regression on the given data in small phases, generalizing them individually, and combining them.

A GLM comprises of the following components [51]:

- Stochastic part (the probability distribution of response variable X).
- Systematic part (the explanatory variable or feature set in this case)
- Link Function (description of link between the stochastic and systematic parts).

The set of all possible outcomes x for a variable X, can be described a using a Probability Mass Function (PMF) given as:

$$p(x) = \binom{n}{x}\pi^x(1-\pi)^{n-x}; \quad \text{for } x = 0, 1, \ldots, n. \tag{7}$$

In our case, there are only two possible outcomes (foreground or background), so this PMF is reduced to a binomial with $n = 1$. The PMF becomes:

$$f(x;\pi) = \pi^x(1-\pi)^{1-x} = (1-\pi)\left[\frac{\pi}{(1-\pi)}\right]^x, \tag{8}$$

$$f(x;\pi) = (1-\pi)\mathrm{e}^{x\log\left(\frac{\pi}{(1-\pi)}\right)}, \tag{9}$$

where the parameter $\log\left(\frac{\pi}{(1-\pi)}\right)$ is a special case of a link function of GLM, also known as the logarithm of the odds, log-odds or logits. This logarithmic parameter forms the log-odds of response 1, the logit of π.

Both CLAHE and GLM are separately used to boost the contrast of pixels and attenuate the intensity of background features. The results from both these preprocessing stages are individually used for segmentation of vessels and compared in Section IV.

C. PROBABILISTIC PATCH-BASED (PPB) DENOISER

Retinal fundus images suffer from the systematic AWGN as well as the multiplicative speckle noise, modeled using the Rayleigh distribution [5]. Therefore, researchers strive to come up with denoisers that could concurrently remove both the additive and multiplicative noise from fundus images [6]–[8]. Yet, the problem persists owing to its complexity, as dealing with AWGN and the speckle simultaneously is a formidable task. Therefore, conventionally both the Gaussian and speckle denoising are performed separately by assuming the relevant noise model, i.e., either AWGN or speckle. To overcome this limitation, AWGN is ignored in cases of mix noise such as the retinal fundus images because speckle has a far worse impact on the structure of these images. Therefore, speckle denoising methods may be more suitable when denoising the retinal fundus images.

In this regard, we propose the use of a state-of-the-art speckle denoising method known as a PPB filter [11], which is popular for preservation of image structure (or details) while taking care of most of the noise. PPB method extends the popular Non-Local Mean (NLM) filter [9] for speckle denoising using the probabilistic maximum likelihood estimation. Other speckle variants of the NLM method employ data-driven approaches to set weights [10], [52]. However, in order to better preserve the textures and edges within the image, PPB assumes Nakagami-Rayleigh distribution model for speckle noise to iteratively estimate the weights for NLM filtering. PPB is also available for suppressing AWGN, but in this work we will only discuss the PPB filter for speckle removal due to its relevance to our work.

Let x_t and s_t denote the noisy and true pixels for any spatial location t, then Weighted Maximum Likelihood Estimation (WMLE) of the parameters $\hat{\theta}_t$ corresponding to the true image, is defined as follows:

$$\hat{\theta}_t = \underset{s_t}{\text{argmax}} \sum_r w(r,t)\log\left(p(x_r|\theta_t)\right), \tag{10}$$

where $w(r,t) \geq 0$ are data driven weights, and $p(x_r|\theta_t)$ is an uncorrelated parametric noise distribution with space varying parameter θ_t.

The definition in (10) for AWGN case, i.e., $\mathcal{N}(s_t, \sigma^2)$ where s_t comprises of the true image pixels, gives a weighted mean averaging solution as follows:

$$\hat{s_t} = \frac{\sum_r w(r,t)x_r}{\sum_r w(r,t)}. \tag{11}$$

According to the first order optimality condition, (11) also maximizes the WMLE ((10)) for the Nakagmi-Rayleigh distribution, given as follows:

$$p(y_t|x_t) = \frac{2l^l}{\Gamma(l)x_t^l}y_t^{2l-1}e^{\left(-\frac{ly_t^2}{x_t}\right)}, \tag{12}$$

where l is the number of looks, and $\Gamma(l)$ denotes the gamma function. In the context of Synthetic Aperture Radar (SAR) image denoising, x_t are considered as magnitudes of the image y_t, i.e., $y_t = \sqrt{x_t}$.

Generally, the choice of weights is key to the success of the weighted averaging filters, as noticed in [9]. An estimation of appropriate weights leads to the preservation of singular features of the noisy image (e.g., vessels in case of retinal images). To this end, PPB approach employs a probabilistic framework that generalizes the Euclidean Distance (ED) based weight estimation. To put things in perspective, ED was used to measure the similarity between two patches within the original NLM filter. On the contrary, the PPB filter estimates similarity between two patches based on their similarity via a probability measure, defined as decaying exponential of the statistical distance between the patches.

For the optimal convergence of WMLE, PPB filter employs an iterative approach based on the probabilistic framework. The reason for the iterative framework within PPB relates to the accuracy of the restored image, and preservation of image singularities or edges. The problem with the existing denoising or despeckling techniques is the lossy nature of these operations, especially in case of speckle removal. The fact that PPB iterative approach uses the knowledge of previous weights to obtain optimum weights, ensures maximization of WMLE and enhanced preservation of image features.

In that context, the iterative estimation of new weights is modeled as a Bayesian estimation problem that incorporates previous weights. Within this definition, the prior term measures the similarity between two patches using the Kullback-Leiber divergence, while the data fidelity term incorporates the properties of the noisy data at hand. That results in following iterative weight estimation procedure:

$$w(r,t)^i = \exp\left[-\sum_k \left(\frac{1}{h}\log\left(\frac{y_{r,k}}{y_{t,k}}+\frac{y_{t,k}}{y_{r,k}}\right)+\frac{l}{T}\frac{|\hat{x}_{r,k}^{i-1}-\hat{x}_{t,k}^{i-1}|}{\hat{x}_{t,k}^{i-1}\hat{x}_{r,k}^{i-1}}\right)\right], \tag{13}$$

where $\hat{x}^{i-1}$ is the estimate of the true image in the previous iteration, while k is the search index within the patches centered at spatial location t and r. If $T \to \infty$, the PPB iterative filter in (13) reduces to the conventional NLM filter.

The iterative procedure responsible for the preservation of image singularities and texture is based on the following two steps: first the similarity between two noisy patches is estimated and subsequently, appropriate weights are assigned to obtain the restored image $\hat{x}^{i-1}$ using the weighted averaging approach in (11). The second step refines the weights iteratively using (13), where the similarity between restored patches from the denoised image (in the previous iteration), is incorporated within the refining process leading to non-local weighted mean filtering using the new weights.

Due to its robust architecture, PPB denoiser yielded enhanced retinal fundus images, where substantial improvement within the low contrast regions containing the smallest of vessels is observed. Consequently, the tiniest of vessels which were previously concealed by noise, were made prominent and clear. This enabled an improved segmentation process, as highlighting these tiny vessels lead to a more accurate mapping of the vessel tree within the retina.

D. MODIFIED FRANGI

A tree-like structure that branches out into smaller nodes is quite similar in anatomy to the vascular entities within the retina. Various filters have been employed for the enhancement of retinal vessels and suppression of other non-vessel features, before the actual detection process could begin. As their response is most prominent around high contrast vessels, these filters exhibit varying deficiencies when differentiating between vessels of different radii and tortuosity. Vessel detection accuracy also fairs badly against challenging areas, such as vessel junctions, edges, and retinal anomalies (hemorrhages, microaneurysms etc.)

Frangi *et al.* [25] employed Hessian matrices to evaluate the 'vessel-ness measure' of any arbitrary geometrical entity. His work took major inspiration from Sato *et al.* [53] and Lorenz *et al.* [54], where the aim was to develop an elliptical and cross-sectional size independent detector. A vessel may appear in various shapes and dimensions, so it is paramount that the detection algorithm is capable of vascular segmentation with an adaptable size threshold. Frangi employed multi-scale ratio Hessian eigenvalues to accomplish better results in segmentation, followed by a notable enhancement in key performance indicators such as sensitivity and specificity. Also, filtering via eigenvalues ratio, helped accomplish contrast independence of objects while imparting the overall process with robustness against the lower magnitude eigenvalues.

The geometric analysis around any arbitrary pixel is well encapsulated by employing a Hessian matrix. This specialized matrix exhibits a strong response towards tubular structures (such as vessels), as compared to other simple and complex geometric entities. Enhancement functions that are targeted towards tube-like structures are scalar in nature, and generally employed on a Gaussian scale space of an image. To augment the local features (i.e., vessels in our case) of varying sizes in an image, this Gaussian scale space proves to be an invaluable tool, as the Gaussian template size can be tuned to match different image spacing in each dimension. This can be further elaborated by the example that, when tube-like structures are dissected and their cross-section area is observed, they exhibit a high intensity in the middle of the cross-section which gradually decays as it moves towards the boundary. A mathematical representation of 2-D Gaussian function can be given as:

$$G(x,y) = \frac{1}{2\pi\sigma^2}e^{-\frac{x^2+y^2}{2\sigma^2}}. \tag{14}$$

The intensity of any tubular feature under consideration, can be included as any constant (e.g., C) times a Gaussian

function, given mathematically as:

$$I_0(x, y, z) = C\ G(x, y) = \frac{1}{2\pi\sigma_\circ^2} e^{-\frac{x^2+y^2}{2\sigma_\circ^2}}. \tag{15}$$

Here σ^2 translates to the variance (or radius of Gaussian), and is analogous to the encapsulation of non-zero values in the evaluation grid of the Gaussian kernel. For example, for a Gaussian kernel having 100×100 pixels, if the variance is going from -5 to $+5$ in both x and y dimensions, the effective grid resolution becomes $(5-(-5))/100 = 0.1$. This value of 0.1 implies that all non-zero values are encapsulated within 10% span of the original kernel. Or, in terms of an image, the pixel that this kernel (of radius 5) convolves on, would only take the influence of 10 of its neighboring pixels (5 from the left and 5 from the right), with the highest influence taken from the center pixel and lowest influence from the ones at the corners. Therefore, the choice of variance is highly application specific. Digital images and the convolution kernels that act upon them, are discrete in nature. A discrete Gaussian kernel approximation can faithfully represent a continuous Gaussian kernel using a greater variance, all be it at a higher computational cost. So, there is a tradeoff between the Gaussian kernel size and the its effective variance.

The retinal vessels width vary between large vessels spanning across 9 pixels, and smaller vessels of 2 pixels. So, this radius selection of the Gaussian kernel plays a crucial role in the detection of vessels of different sizes. A Gaussian filter also exhibits circular symmetry i.e., a 2-D Gaussian kernel can be implemented as two 1-D Gaussian kernels. The same 1-D kernels are used in modified Frangi filter, using three parameters known as sigma(σ), spacing, and size. Sigma defines the Gaussian kernel's radius of influence (variance), spacing gives the input image spacing used to adjust the size of the Gaussian kernel, and size depicts the Gaussian kernel size (area over which averaging of pixels occur, 6*Sigma for our case). These three parameters control the size of the vessels the detector aims to find. There was no concept of spacing in the original Frangi method, whereas the modified Frangi method keeps sigma constant while varying the spacing to deal with different resolution images. So, if a spacing of 1 is used, the overall spread goes from -6 to $+6$, which in turn, will start detecting vessels of width 12. If the spacing is increased to 2, the span of the detector goes from -3 to $+3$, thereby detecting vessels that are 6 pixels wide. Similarly, if the spacing is taken as 6, the kernel span goes from -1 to $+1$, effectively tuning the detector to track vessels of a pixel width of 2. That way, keeping the Gaussian kernel size constant, and varying the spacing parameter, vessels of different sizes can be segmented individually.

A square matrix of the second-order partial derivative of a range of data that is scalar, forms a Hessian matrix also known as a Hessian. Let $I(x)$ represent the intensity at pixel location $x = (x_1, x_2, \ldots, x_N)^T$ of a N-dimensional image. A matrix of dimensions $N \times N$ holds the Hessian of $I(.)$ responses at scale s, which is given as follows,

$$H_{ij}(x, s) = s^2(x)\frac{\partial^2}{\partial x_i \partial x_j} G(x, s), \tag{16}$$

where $i, j = 1, 2, 3, \ldots, N$. Also, $G(x, s)$ is a N-variate Gaussian given by:

$$G(x, s) = (2\pi s^2)^{-D/2} e^{\frac{-x^T x}{2s^2}}. \tag{17}$$

The determinants of the Hessian matrices describe how a function behaves about the point under consideration, by yielding its trademark Hessian binary output of either 1 for a local maximum and 0 for a local minimum. This point is of particular importance in image processing as it describes a pixel's influence on its neighbors or vice versa. A Hessian matrix employing partial differentials of second order, is formed as:

$$H = \begin{pmatrix} I_{xx} & I_{xy} \\ I_{yx} & I_{yy} \end{pmatrix}, \tag{18}$$

where the matrix elements above constitute the second partial derivatives from the intensity profile of the host image and are used to calculate two eigenvalues labeled as λ_1 and λ_2. These eigenvalues are ordered such that $|\lambda_1| < |\lambda_2|$, and a vesselness likelihood parameter for every pixel is calculated and sorted based on the pixel ratio response.

$$V(s) = \begin{cases} 0; & \lambda_2 > 0 \\ \exp\left(-\frac{{R_B}^2}{2\beta^2}\right)\left(1 - \exp\left(\frac{s^2}{2c^2}\right)\right); & \lambda_2 \leq 0, \end{cases} \tag{19}$$

$$R_B = \frac{|\lambda_1|}{|\lambda_2|}, \quad S = \sqrt{{\lambda_1}^2 + {\lambda_2}^2}. \tag{20}$$

The maximum points of every pixel are selected to yield the overall Frangi filter response. The parameter s in 19, is the scaling factor ranging from 1 to 5, and the value of c is used to configure its sensitivity. Similarly, β is used in 19 to tune the sensitivity of the parameter R_B.

The popularity of the Frangi filter comes from the fact that, it exhibits a near-uniform reaction to all geometric entities with the same intensity profile. The same uniform reaction turns into a disadvantage as having the magnitude of the eigenvalues at the Frangi filter's core, makes it unsuitable for objects such as vessels which have a higher contrast disparity along their length as well as width. Experimentation with the above vessel-like measure showed that it responds strongly at the core of the vessel and lessens abruptly when moving away from the middle.

It is a highly undesirable trait for any vascular segmentation algorithm that focuses on boundary pixels for making a clear distinction between a vessel's edge and the background. A solution to this problem was suggested in [55], by using specialized virtual ratios of multi-scale Hessian eigenvalues. A review by Jerman *et al.* [56], elaborates on many enhancement techniques some of which can act upon a similar

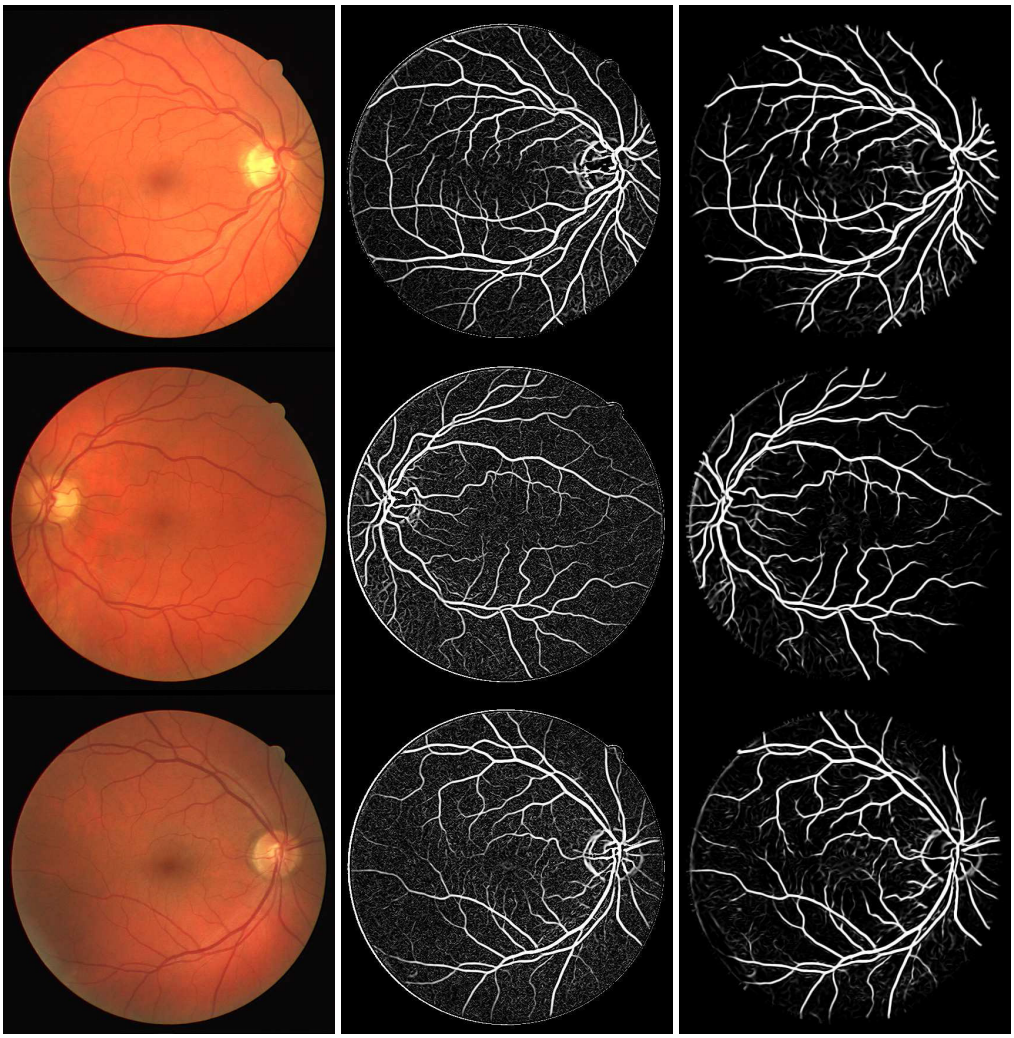

(a) (b) (c)

FIGURE 3. Analysis of modified Frangi output of three sample images (test image 2, 5, 10) of the DRIVE dataset: (a) original image, (b) output of simple Frangi method, and (c) modified Frangi method.

Hessian matrix. One such method is Volume Ratio (VR), having its eigenvalues response stretched from a preset threshold to either a 0 and 1. VR, as suggested in 21, is employed for spherical diffusion tensors detection. It is further adapted by adding a factor of $\lambda_1 = \lambda_2 - \lambda_1$ to incorporate both stretched out and spherical structures. If $\lambda_0, \lambda_1, \lambda_2, \cdots, N$ represents the eigenvalues of a Hessian matrix of order N, VR is further elaborated as:

$$VR = \lambda_1\lambda_2\lambda_3\left[\frac{3}{(\lambda_1+\lambda_2+\lambda_3)}\right]^2. \tag{21}$$

The ratios were set up to develop another vesselness likelihood parameter V_p, having a near-uniform reaction to vessels of all shapes and sizes along with more efficient foreground to background differentiation. Similarly, other ratios were tested to achieve a higher accuracy and balanced enhancement in all kinds and sizes of vessels, along with superior edge and endpoint contrast improvements. All this, unified into a stand-alone enhancement procedure, is given by:

$$V_p = \begin{cases} 0; & \lambda_2 > 0 \wedge \lambda_3 > 0, \\ 1; & \lambda_2 \leq \lambda_p/2, \\ \lambda_2^2\left(\lambda_p - \lambda_2\right)\left(\dfrac{3}{\lambda_2+\lambda_p}\right)^3; & \text{otherwise.} \end{cases} \tag{22}$$

The final ratio is disproportional to all its constituent eigenvalues along with being immune to eigenvalues of lower magnitudes. These crucial features help alleviate the contrast disparity problem and pave the way for a more precise and robust vascular segmentation, as depicted in Fig. 3 and Fig. 4.

This response closely follows the visualization of the vessel content among varying contrast of raw image intensities. Vessel enhancement filters were computed on a scale of $sc_{min} = 0.5$ to $sc_{max} = 2.5$ mm, with step size of 0.5 mm over this range. The same range was used for testing on all images of the clinical dataset.

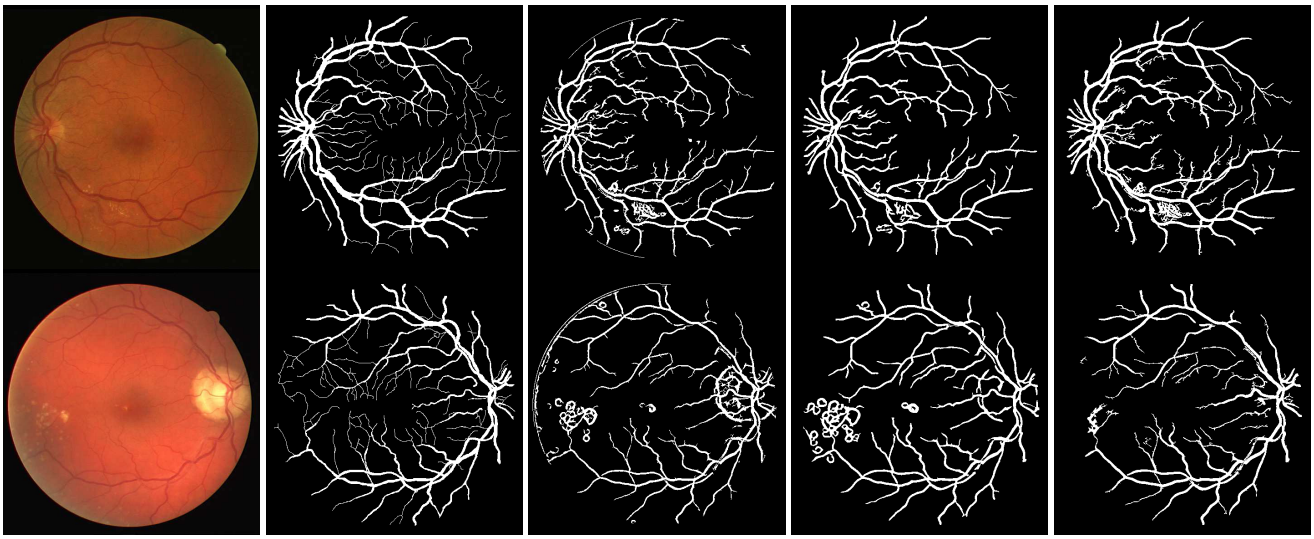

FIGURE 4. Analysis of binarized output of two sample images (images 3 and 8) of the DRIVE dataset: (a) input image, (b) ground truth image, (c) output of simple Frangi method, (d) modified Frangi method without tiny vessel enhancement and denoiser, and (e) proposed method with tiny vessels.

E. BINARIZATION

Image binarization is a non-linear operation that converts every pixel of an image into just two tones, black and white. In image segmentation, these two levels of black and white are usually associated with background and foreground, respectively. The retinal images that are acquired from the color to gray-scale conversion, still contain overlapping vessel and non-vessel regions after passing through various image processing steps. So, a thresholding operation is necessary to clearly differentiate vessel pixels from the background. This is done by selecting an intelligent threshold value, which bifurcates all pixels in the image into two levels, i.e., foreground (white) and background (black).

The selection of the threshold value can be done on a local or global scale. It is done by counting the occurrence of each gray-level in an area or region of interest, and setting the threshold based on this data. The Ridler-Calvard's Iterative-Selection (IS) technique [57], also known as IsoData algorithm, is one such method that is used to find an optimum global threshold for image binarization. It uses the histogram of the image to scan for the smallest continuous range of gray levels with non-zero frequency. Let $[L_1, L_2]$ denote the endpoints of this non-zero interval on the histogram, then the IsoData algorithm is elaborated as:

1) Select a starting value for the mean using the inequality equation $L_1 \leq \mu \leq L_2$. In this study, the starting value of mean is calculated from the Otsu method.
2) Evaluate the binarization threshold T_M by:

$$T_M = \frac{\mu_0 + \mu_1}{2}. \tag{23}$$

This T_M is used to bifurcate the image pixels into vessels and background.

3) Two new mean values, μ_0 and μ_1 are calculated, depending upon new boundaries formed by T_M.
4) If either of the two mean values change, loop to 2; else stop.

The initial value of the threshold T_M is selected by choosing a region comprising of predominantly background pixels. After evaluating the histogram, threshold is set at a fixed offset under the max valued bin. A more refined approach involves adding the histogram bin counts from the max value and working downwards. Set the threshold after the accumulation of some fixed portion of the total population (0.1%).

IV. EXPERIMENTAL RESULTS

This section presents the results obtained from conducted experimental evaluations. Moreover, a thorough analysis on the obtained results is also conducted.

A. MATERIALS

The planned technique was put to the test using two sets of figures accessible publicly as listed below:

1) DRIVE [18], Digital Retinal Images for Vessel Extraction: Retinal scans taken from a broad age group diabetics in the Netherlands.
2) STARE [15] STructured Analysis of the REtina: 20 samples from a collection of 400 mid-resolution images, taken in the USA.

The images from the DRIVE dataset have a resolution of 768 × 584 pixels. 20 retinal images are taken from DRIVE accompanied by their binary masks. A binary mask is a vessel/non-vessel oriented Boolean image, in which the vascular structure has been manually annotated by an expert. A total of 20 images have also been used from the STARE dataset, each having a resolution of 700 × 605 pixels.

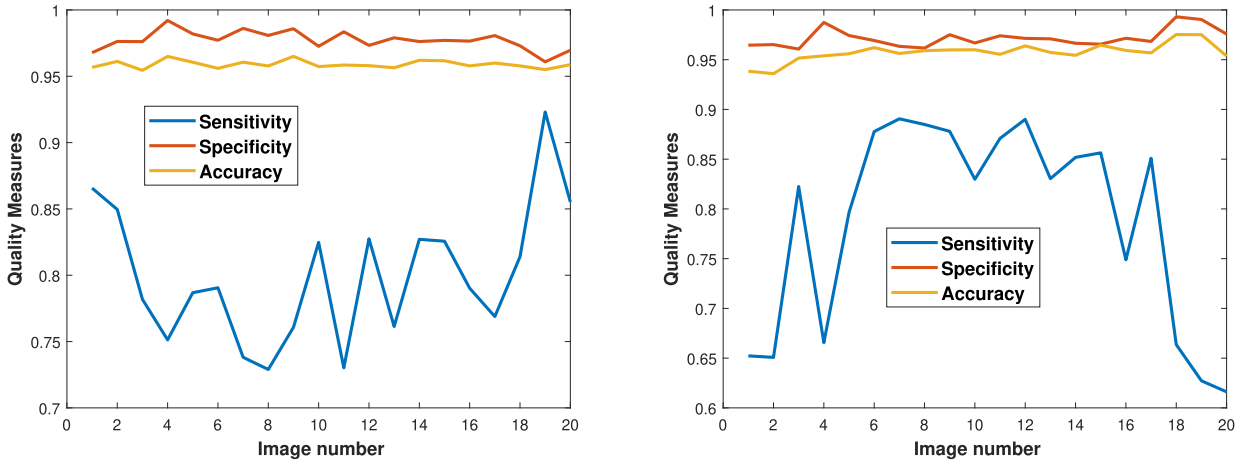

FIGURE 5. Quality measures of the propoposed method with GLM for datasets: (a) on DRIVE, (b) on STARE.

The different thing about STARE is that, it comprises of 10 normal and 10 pathological retinal images that present an added challenge in the form of detecting vessels in the presence of retinal anomalies.

The availability of masks and ground truth images for both these datasets make them ideal candidates to validate our algorithm. The use of images from these datasets is fairly common in literature, therefore, it also provides a good opportunity to contrast the performance of our proposed methodology with other existing methods.

B. EVALUATION CRITERION

The efficiency of any vascular segmentation methodology relies on its ability to correctly discriminate between vessels and the background pixels. The performance metrics are evolved by comparing the segmentation results with the manually annotated ground truth binary masks that act as the reference maps. This comparison yields the core values of true/false and positive/negative. A pixel identified as a vessel is labeled positive, while recognition as a background pixel puts it in the false category. True implies correct segmentation of any pixel as either vessel or non-vessel and vice versa. So, all four combinations of these variables play an important role in determining the efficacy of any vascular classification technique, and are further elaborated as follows:

1) True Positive (TP): Vessels classified correctly.
2) False Negative (FN): Vessels classified as background.
3) True Negative (TN): Non-vessels classified correctly.
4) False Positive (FP): Non-vessels classified as vessels.

Using the core parameters listed above, specific ratios are evaluated to quantify and contrast the performance of the technique under scrutiny with other state-of-the-art segmentation strategies as follows [39]:

$$\text{Sensitivity(Sn)} = \frac{TP}{TP + FN}, \tag{24}$$

$$\text{Specificity(Sp)} = \frac{TN}{TN + FP}, \tag{25}$$

$$\text{Accuracy(Acc)} = \frac{TP + TN}{TP + FN + TN + FP}. \tag{26}$$

A high *Sn* measure or True Positive Rate (TPR), indicates a better vessel segmentation ability, and the same goes for *Sp* (or 1-FPR) in terms of classifying the background pixels. The ratio of all pixels rightly classified as either vessels or background with the total pixels inside the Field Of View (FOV), yields the accuracy of the algorithm. Accuracy is therefore, the ratio of all correctly classified pixels (pixels and background) with all the pixels in that image. Another performance measure is the AUC, known as area under the Receiver Operating Characteristic (ROC) curve. It is calculated by observing the ROC under varying threshold conditions. AUC does not apply to our method as we treat the segmentation of large and tiny vessels as separate binarization problems, which are later linearly combined to produce the overall segmentation result.

C. COMPARISON WITH STATE-OF-THE-ART

For comparison with the latest vessel detection methods, experiments were conducted on DRIVE and STARE datasets, and their performance evaluation metrics were gauged. Individual image-based performance parameters are listed in Fig. 5. Results in Fig. 6 and Fig. 7 give a visible indication of the advantages the size-oriented vessel segmentation through the proposed methodology. An objective comparison follows in the forms of tables 1 and 2 where the performance parameters are compared with other top vessel segmentation strategies. Fig. 8 depicts the effectiveness of the method in retinal images with pathologies.

The proposed methodology, employing the simple Frangi vessel detector, was tested on DRIVE dataset resulting in a good *Sp* score of 0.9745, but Sn was still weak at 0.7205. Highest *Sn* scores (CLAHE=0.8027, GLM=0.7907) are

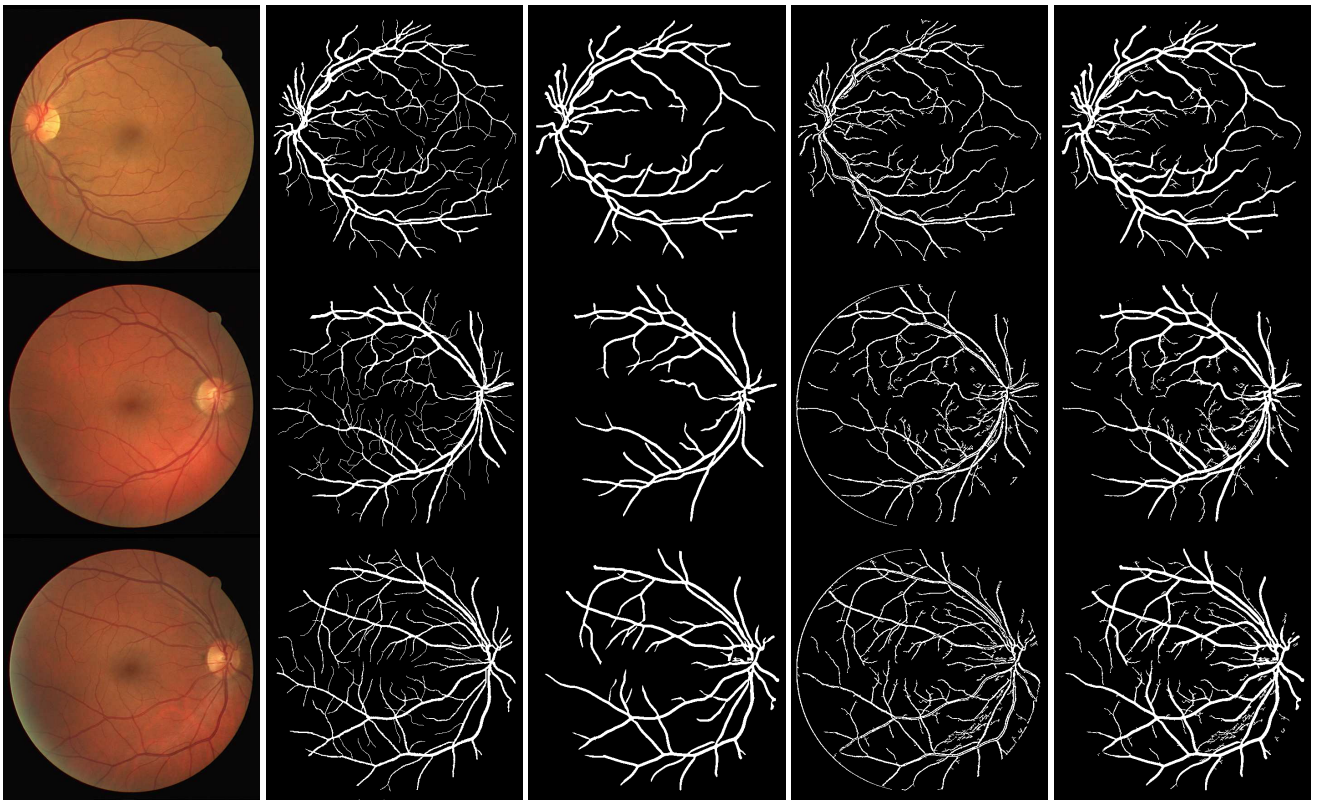

FIGURE 6. Analysis of binarized output of three sample images (images 1, 10 and 19) of the DRIVE dataset using GLM: (a) input image, (b) ground truth image, (c) large vessel segmentation, (d) tiny vessel segmentation, and (e) combined binarized output.

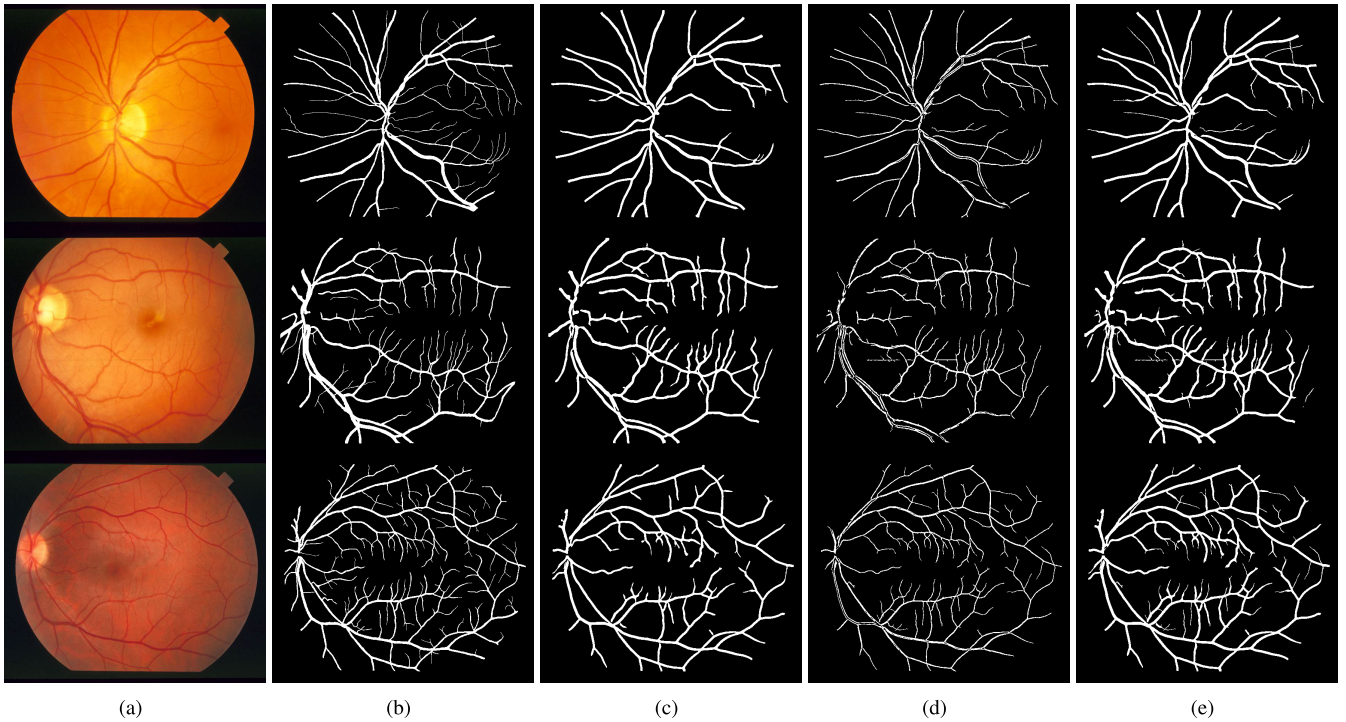

FIGURE 7. Analysis of binarized output of three sample images (images 12, 14 and 17) of the STARE dataset using GLM: (a) input image, (b) ground truth image, (c) large vessel segmentation, (d) tiny vessel segmentation, and (e) combined binarized output.

TABLE 1. Comparison with the most recent techniques on the DRIVE dataset.

Type	Methods	Year	Sn	Sp	Acc
Supervised methods	Marin [22]	2011	0.7067	0.9801	0.9452
	Fraz [58]	2012	0.7406	0.9807	0.948
	Cheng [59]	2014	0.7252	0.9798	0.9474
	Li [60]	2016	0.7569	0.9816	0.9527
	Orlando FC [61]	2017	0.7893	0.9792	N.A
	Orlando UP [61]	2017	0.7076	0.987	N.A
	Dasgupta [62]	2017	0.9691	0.9801	0.9533
	Yan [63]	2018	0.7653	0.9818	0.9542
Unsupervised methods	Zhang [64]	2010	0.776	0.8724	0.9472
	Lam [65]	2010	N.A	N.A	0.9472
	Miri [66]	2011	0.7352	**0.9795**	0.9458
	Fraz [67]	2011	0.7152	0.9759	0.943
	You [68]	2011	0.741	0.9751	0.9434
	Azzopardi [69]	2015	0.7655	0.9704	0.9442
	Roychowdhury [20]	2015	0.7395	**0.9782**	0.9494
	Yin [70]	2015	0.7246	**0.979**	0.9403
	Zhang [71]	2016	0.7743	0.9725	0.9476
	Neto [72]	2017	**0.7806**	0.9629	0.8718
	Soomro [73]	2018	0.745	0.962	0.948
	Khan [43]	2018	0.7696	0.9651	0.9506
	Chalakkal [47]	2019	0.7653	0.9735	**0.9542**
	Proposed Method (CLAHE)	2019	**0.8027**	0.9733	**0.9561**
	Proposed Method (GLM)	2019	**0.7907**	**0.979**	**0.9603**

TABLE 2. Comparison with state-of-the-art methods on the STARE dataset.

Type	Methods	Year	Sn	Sp	Acc
Supervised methods	Marin [22]	2011	0.6944	0.9819	0.9526
	Fraz [58]	2012	0.7548	0.9763	0.9534
	Li [60]	2016	0.7726	0.9844	0.9628
	Orlando FC [61]	2017	0.768	0.9738	N.A
	Orlando UP [61]	2017	0.7692	0.9675	N.A
	Yan [63]	2018	0.7581	0.9846	0.9612
Unsupervised methods	Zhang [64]	2010	0.7177	0.9753	0.9484
	Fraz [67]	2012	0.7311	0.968	0.9442
	You [68]	2011	0.736	0.9756	0.9497
	Azzopardi [69]	2015	0.7716	0.9701	0.9497
	Roychowdhury [20]	2015	0.7317	**0.9842**	**0.956**
	Yin [70]	2015	**0.8541**	0.9419	0.9325
	Zhang [71]	2016	0.7791	0.9758	0.9554
	Neto [72]	2017	**0.8344**	0.9443	0.8894
	Soomro [73]	2018	0.784	**0.976**	0.951
	Khan [43]	2018	0.7521	**0.9812**	0.9513
	Proposed method (CLAHE)	2019	**0.798**	0.9732	**0.9561**
	Proposed Method (GLM)	2019	0.786	0.9725	**0.9583**

achieved on DRIVE with the proposed method. Competitive *Sn* scores are established for STARE as well, scoring 0.798 for CLAHE and 0.7860 for GLM at the preprocessing stage, respectively. Similarly, the *Sp* scores for CLAHE (0.9733, 0.9732) and GLM (0.9732, 0.9725) are achieved for DRIVE and STARE, respectively. The GLM preprocessing strategy yields the highest accuracy scores of 0.9603 and 0.9583 for the DRIVE and STARE databases, respectively. Accuracy with CLAHE stands second best in both repositories, with scores of 0.9561 and 0.9561 for the DRIVE and

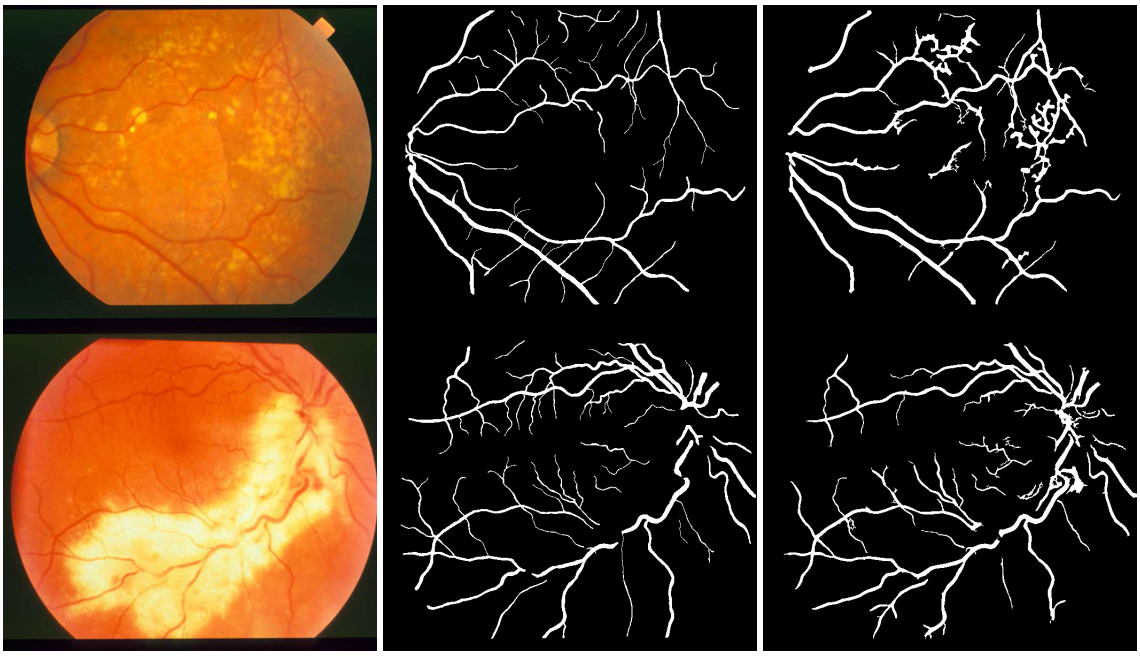

(a) (b) (c)

FIGURE 8. Analysis of proposed method on pathological images (images 3 and 6) of the STARE dataset: (a) original image, (b) ground truth image, and (c) proposed method.

TABLE 3. Average time for processing one image.

Method	Computation Time	Hardware Specifications	Software
Mendonca [30]	2.5 to 3 mins	Pentium-4, 3.2 GHz, 960 MB RAM	MATLAB
Soares [19]	2 mins (9 hours for training)	Pentium-4, 2.1 GHz, 1 GB RAM	MATLAB
Lam [65]	13 mins	Core 2 Duo 1.83 GHz, 2 GB RAM	MATLAB
Staal [17]	15 mins	Pentium-3, 1 GHz, 1 GB RAM	N. A.
Zhao [74]	22 sec	Core i-3 CPU, 2.53 GHz, 4 GB RAM	MATLAB, C
Proposed	**75 sec**	**Core i7 CPU 2.21 GHz, 16 GB RAM**	**MATLAB**

STARE database, respectively. The results in these tables are ranked by a color-coding scheme such that, red, green, and blue colors signify the top, second and third ranked methods in that particular category, respectively. The computation times for the proposed methodology are contrasted against other techniques in literature in table 3.

Considering the DRIVE dataset, the proposed method reports a substantial improvement in *Sn* scores (CLAHE=0.8027, GLM=0.7907) of all unsupervised methods followed by Neto *et al.* [72] (0.7806). The proposed method matches the Sp of top performers Miri and Mahloojifar [66] (0.9795) and Yin *et al.* [70] (0.9790), yet it is pertinent to note here that both these methods sacrificed other parameters to achieve these *Sp* scores. The accuracy scores (GLM=0.9603, CLAHE=0.9561) show an improvement over the third place Chalakkal and Abdulla [47] (0.9542). It can be concluded that with the Sp and Acc measures closely matching that of the best methods, the proposed method outperforms all the state-of-the-art methods in *Sn*.

For the STARE database, the thresholding technique is employed to generate the FOV masks used for performance evaluation. The proposed method reports modest *Sn* (CLAHE=0.798, GLM=0.7860) and *Sp* (CLAHE=0.7932, GLM=0.9725) scores that are comparable with the top contenders in each of their respective categories. It is also noteworthy here that, other techniques post high scores in individual categories at the cost of other performance parameters. Importantly, in terms of accuracy, both variations of our method register a substantial improvement (GLM=0.9583, CLAHE=0.9561) upon the third place Roychowdhury *et al.* [20] (0.9560).

Overall, it can be deduced from the discussion above that, both variations of the proposed method yield competitive key performance indicators that are seldom at par and mostly pull

ahead of the state-of-the art techniques. Adding the denoiser phase before vessel detection improves the accuracy of the modified Frangi method, particularly with respect to the tiny vessels that cause the bulk of false positives and are most difficult to segment out.

V. CONCLUSION

Refining the vessel map in retinal fundus images helps with the visualization and automatic segmentation of the vessels, thus paving the way for further anatomical and pathological scrutiny of the retina. The ratio of multi-scale Hessian re-construction of an image is an extremely potent tool for detecting tubular structures similar to blood vessels, but it relies on a vibrant contrast for it to work efficiently. Contrast enhancement, on the other hand, exhibits a tradeoff between improving the contrast and keeping the noise amplification to a minimum. SVD does a brilliant job at improving the vessel contrast, but also adds considerable noise to an image.

In this paper, we have devised a new strategy by introducing a denoiser that precedes the vessel segmentation step to mitigate the noise spike caused by SVD. This step significantly boosts the efficiency of Frangi vessel detection capabilities. Two contrast normalization steps (CLAHE and GLM) are tested to gauge the effects of preprocessing phase on the overall segmentation process. Modified Frangi, individually tuned for large and tiny vessels, further refines the performance parameters with excellent scores for *Sn* (CLAHE=0.8027, 0.798; GLM=0.7907, 0.7860) and *Acc* (CLAHE= 0.9561,0.9561; GLM=0.9603, 0.9583).

The proposed method is tested on well-established clinical datasets and surpassed the state-of-the-art methods with significant enhancement, especially in the detection accuracy. This is the first time modified Frangi method has been used in sync with a denoiser for vessel segmentation, and the tackling of noise enhancement during contrast improvement has also not been used in any other application. A drawback of this method comes in the form of a relatively hefty computational time of 77 seconds, a big chunk of which is taken by the denoiser phase. However, real-time constraints do not apply strictly to the task of vessel segmentation. Future works may see the application of the PPB denoiser in additional line detectors, as well as various other segmentation techniques to investigate its impact on their efficiency.

REFERENCES

[1] H. M. Pakter, E. Ferlin, S. C. Fuchs, M. K. Maestri, R. S. Moraes, G. Nunes, L. B. Moreira, M. Gus, and F. D. Fuchs, "Measuring arteriolar-to-venous ratio in retinal photography of patients with hypertension: Development and application of a new semi-automated method," *Amer. J. Hypertension*, vol. 18, no. 3, pp. 417–421, 2005.

[2] T. A. Soomro, J. Gao, T. M. Khan, A. F. M. Hani, M. A. U. Khan, and M. Paul, "Computerised approaches for the detection of diabetic retinopathy using retinal fundus images: A survey," *J. Pattern Anal. Appl.*, vol. 20, no. 4, pp. 927–961, 2017.

[3] A. A. G. Elseid, M. E. Elmanna, and A. O. Hamza, "Evaluation of spatial filtering techniques in retinal fundus images," *Amer. J. Artif. Intell.*, vol. 2, no. 2, p. 16, 2018.

[4] K. B. Khan, A. A. Khaliq, A. Jalil, M. A. Iftikhar, N. Ullah, M. W. Aziz, K. Ullah, and M. Shahid, "A review of retinal blood vessels extraction techniques: Challenges, taxonomy, and future trends," *Pattern Anal. Appl.*, vol. 22, no. 3, pp. 767–802, 2019.

[5] A. F. M. Hani, T. A. Soomro, I. Fayee, N. Kamel, and N. Yahya, "Identification of noise in the fundus images," in *Proc. IEEE Int. Conf. Control Syst., Comput. Eng.*, Nov./Dec. 2013, pp. 191–196.

[6] P. Dai, H. Sheng, J. Zhang, L. Li, J. Wu, and M. Fan, "Retinal fundus image enhancement using the normalized convolution and noise removing," *Int. J. Biomed. Imag.*, vol. 2016, Aug. 2016, Art. no. 5075612.

[7] A. F. M. Hani, T. A. Soomro, I. Faye, N. Kamel, and N. Yahya, "Denoising methods for retinal fundus images," in *Proc. 5th Int. Conf. Intell. Adv. Syst. (ICIAS)*, Jun. 2014, pp. 1–6.

[8] I. Jamal, M. U. Akram, and A. Tariq, "Retinal image preprocessing: Background and noise segmentation," *Telkomnika*, vol. 10, no. 3, pp. 537–544, 2012.

[9] A. Buades, B. Coll, and J.-M. Morel, "A non-local algorithm for image denoising," in *Proc. IEEE Comput. Soc. Conf. Comput. Vis. Pattern Recognit. (CVPR)*, vol. 2, Jun. 2005, pp. 60–65.

[10] G. D. Martino, A. D. Simone, A. Iodice, and D. Rioccio, "Scattering-based nonlocal means SAR despeckling," *IEEE Trans. Geosci. Remote Sens.*, vol. 54, no. 6, pp. 3574–3588, Jun. 2016.

[11] C.-A. Deledalle, L. Denis, and F. Tupin, "Iterative weighted maximum likelihood denoising with probabilistic patch-based weights," *IEEE Trans. Image Process.*, vol. 18, no. 12, pp. 2661–2672, Dec. 2009.

[12] N. ur Rehman, K. Naveed, S. Ehsan, and K. McDonald-Maier, "Multi-scale image denoising based on goodness of fit (GOF) tests," in *Proc. 24th Eur. Signal Process. Conf. (EUSIPCO)*, Aug./Sep. 2016, pp. 1548–1552.

[13] K. Naveed, B. Shaukat, S. Ehsan, K. D. Mcdonald-Maier, and N. ur Rehman, "Multiscale image denoising using goodness-of-fit test based on EDF statistics," *PLoS ONE*, vol. 14, no. 5, 2019, Art. no. e0216197.

[14] K. Naveed, S. Ehsan, K. D. McDonald-Maier, and N. ur Rehman, "A multiscale denoising framework using detection theory with application to images from CMOS/CCD sensors," *Sensors*, vol. 19, no. 1, p. 206, 2019.

[15] A. D. Hoover, V. Kouznetsova, and M. Goldbaum, "Locating blood vessels in retinal images by piecewise threshold probing of a matched filter response," in *Proc. AMIA Symp.*, 1998, p. 931.

[16] M. M. Fraz, P. Remagnino, A. Hoppe, B. Uyyanonvara, A. R. Rudnicka, C. G. Owen, and S. A. Barman, "Blood vessel segmentation methodologies in retinal images—A survey," *Comput. Methods Programs Biomed.*, vol. 108, no. 1, pp. 407–433, 2012.

[17] J. Staal, M. D. Abramoff, M. Niemeijer, M. A. Viergever, and B. van Ginneken, "Ridge-based vessel segmentation in color images of the retina," *IEEE Trans. Med. Imag.*, vol. 23, no. 4, pp. 501–509, Apr. 2004.

[18] M. Niemeijer, J. Staal, B. van Ginneken, M. Loog, and M. Abramoff, "Comparative study of retinal vessel segmentation methods on a new publicly available database," *Proc. SPIE*, vol. 5370, pp. 648–657, May 2004.

[19] J. V. B. Soares, J. J. G. Leandro, R. M. Cesar, H. F. Jelinek, and M. J. Cree, "Retinal vessel segmentation using the 2-D Gabor wavelet and supervised classification," *IEEE Trans. Med. Imag.*, vol. 25, no. 9, pp. 1214–1222, Sep. 2006.

[20] S. Roychowdhury, D. D. Koozekanani, and K. K. Parhi, "Blood vessel segmentation of fundus images by major vessel extraction and subimage classification," *IEEE J. Biomed. Health Inform.*, vol. 19, no. 3, pp. 1118–1128, May 2015.

[21] E. Ricci and R. Perfetti, "Retinal blood vessel segmentation using line operators and support vector classification," *IEEE Trans. Med. Imag.*, vol. 26, no. 10, pp. 1357–1365, Oct. 2007.

[22] D. Marín, A. Aquino, M. E. Gegúndez-Arias, and J. M. Bravo, "A new supervised method for blood vessel segmentation in retinal images by using gray-level and moment invariants-based features," *IEEE Trans. Med. Imag.*, vol. 30, no. 1, pp. 146–158, Jan. 2011.

[23] R. Nekovei and Y. Sun, "Back-propagation network and its configuration for blood vessel detection in angiograms," *IEEE Trans. Neural Netw.*, vol. 6, no. 1, pp. 64–72, Jan. 1995.

[24] G. E. Hinton, N. Srivastava, A. Krizhevsky, I. Sutskever, and R. R. Salakhutdinov, "Improving neural networks by preventing co-adaptation of feature detectors," 2012, *arXiv:1207.0580*. [Online]. Available: https://arxiv.org/abs/1207.0580

[25] A. F. Frangi, W. J. Niessen, K. L. Vincken, and M. A. Viergever, "Multiscale vessel enhancement filtering," in *Proc. Int. Conf. Med. Image Comput. Comput.-Assist. Intervent.* Berlin, Germany: Springer, 1998, pp. 130–137.

[26] G. Azzopardi and N. Azzopardi, "Trainable COSFIRE filters for keypoint detection and pattern recognition," *IEEE Trans. Pattern Anal. Mach. Intell.*, vol. 35, no. 2, pp. 490–503, Feb. 2013.

[27] M. M. Fraz, R. A. Welikala, A. R. Rudnicka, C. G. Owen, D. Strachan, and S. A. Barman, "QUARTZ: Quantitative analysis of retinal vessel topology and size—An automated system for quantification of retinal vessels morphology," *Expert Syst. Appl.*, vol. 42, no. 20, pp. 7221–7234, 2015.

[28] R. Annunziata, A. Garzelli, L. Ballerini, A. Mecocci, and E. Trucco, "Leveraging multiscale hessian-based enhancement with a novel exudate inpainting technique for retinal vessel segmentation," *IEEE J. Biomed. Health Inform.*, vol. 20, no. 4, pp. 1129–1138, Jul. 2016.

[29] E. Emary, H. M. Zawbaa, A. E. Hassanien, and B. Parv, "Multi-objective retinal vessel localization using flower pollination search algorithm with pattern search," *Adv. Data Anal. Classification*, vol. 11, no. 3, pp. 611–627, Sep. 2017.

[30] A. M. Mendonca and A. Campilho, "Segmentation of retinal blood vessels by combining the detection of centerlines and morphological reconstruction," *IEEE Trans. Med. Imag.*, vol. 25, no. 9, pp. 1200–1213, Sep. 2006.

[31] M. M. Fraz, A. Basit, and S. Barman, "Application of morphological bit planes in retinal blood vessel extraction," *J. Digit. Imag.*, vol. 26, no. 2, pp. 274–286, 2013.

[32] E. M. Sigurðsson, S. Valero, J. A. Benediktsson, J. Chanussot, H. Talbot, and E. Stefánsson, "Automatic retinal vessel extraction based on directional mathematical morphology and fuzzy classification," *Pattern Recognit. Lett.*, vol. 47, pp. 164–171, Oct. 2014.

[33] E. Imani, M. Javidi, and H.-R. Pourreza, "Improvement of retinal blood vessel detection using morphological component analysis," *Comput Methods Programs Biomed.*, vol. 118, no. 3, pp. 263–279, Mar. 2015.

[34] S. Chaudhuri, S. Chatterjee, N. Katz, M. Nelson, and M. Goldbaum, "Detection of blood vessels in retinal images using two-dimensional matched filters," *IEEE Trans. Med. Imag.*, vol. MI-8, no. 3, pp. 263–269, Sep. 1989.

[35] M. Al-Rawi, M. Qutaishat, and M. Arrar, "An improved matched filter for blood vessel detection of digital retinal images," *Comput. Biol. Med.*, vol. 37, no. 2, pp. 262–267, 2007.

[36] M. H. A. Fadzil, L. I. Izhar, P. A. Venkatachalam, and T. Karunakar, "Extraction and reconstruction of retinal vasculature," *J. Med. Eng. Technol.*, vol. 31, no. 6, pp. 435–442, 2007.

[37] Y. Q. Zhao, X. H. Wang, X. F. Wang, and F. Y. Shih, "Retinal vessels segmentation based on level set and region growing," *Pattern Recognit.*, vol. 47, no. 7, pp. 2437–2446, 2014.

[38] B. Dizdaroğlu, E. Ataer-Cansizoglu, J. Kalpathy-Cramer, K. Keck, M. F. Chiang, and D. Erdogmus, "Structure-based level set method for automatic retinal vasculature segmentation," *EURASIP J. Image Video Process.*, vol. 2014, no. 1, 2014, Art. no. 39.

[39] J. Zhang, E. Bekkers, S. Abbasi, B. Dashtbozorg, and B. ter Haar Romeny, "Robust and fast vessel segmentation via Gaussian derivatives in orientation scores," in *Proc. Int. Conf. Image Anal. Process.* Cham, Switzerland: Springer, 2015, pp. 537–547.

[40] R. Panda, N. B. Puhan, and G. Panda, "New binary Hausdorff symmetry measure based seeded region growing for retinal vessel segmentation," *Biocybernetics Biomed. Eng.*, vol. 36, no. 1, pp. 119–129, 2016.

[41] T. A. Soomro, M. A. U. Khan, J. Gao, T. M. Khan, and M. Paul, "Contrast normalization steps for increased sensitivity of a retinal image segmentation method," *J. Signal Image Video Process.*, vol. 11, no. 8, pp. 1509–1517, 2017.

[42] M. A. U. Khan, T. M. Khan, D. G. Bailey, and O. Kittaneh, "Deriving scale normalisation factors for a GLoG detector," *IET Image Process.*, vol. 12, no. 9, pp. 1673–1682, 2018.

[43] M. A. U. Khan, T. M. Khan, D. G. Bailey, and T. A. Soomro, "A generalized multi-scale line-detection method to boost retinal vessel segmentation sensitivity," *Pattern Anal. Appl.*, vol. 22, no. 3, pp. 1177–1196, 2019.

[44] T. A. Soomro, T. M. Khan, M. A. U. Khan, J. Gao, M. Paul, and L. Zheng, "Impact of ICA-based image enhancement technique on retinal blood vessels segmentation," *IEEE Access*, vol. 6, pp. 3524–3538, 2018.

[45] K. B. Khan, A. A. Khaliq, A. Jalil, and M. Shahid, "A robust technique based on VLM and Frangi filter for retinal vessel extraction and denoising," *PLoS ONE*, vol. 13, no. 2, Feb. 2018, Art. no. e0192203, doi: 10.1371/journal.pone.0192203.

[46] M. Shahid and I. A. Taj, "Robust retinal vessel segmentation using vessel's location map and Frangi enhancement filter," *IET Image Process.*, vol. 12, no. 4, pp. 494–501, Apr. 2018.

[47] R. J. Chalakkal and W. H. Abdulla, "Improved vessel segmentation using curvelet transform and line operators," in *Proc. Asia–Pacific Signal Inf. Process. Assoc. Annu. Summit Conf. (APSIPA ASC)*, Nov. 2018, pp. 2041–2046.

[48] U. T. V. Nguyen, A. Bhuiyan, L. A. F. Park, and K. Ramamohanarao, "An effective retinal blood vessel segmentation method using multi-scale line detection," *Pattern Recognit.*, vol. 46, no. 3, pp. 703–715, 2013.

[49] K. Zuiderveld, "Contrast limited adaptive histogram equalization," in *Graphics Gems IV*. New York, NY, USA: Academic, 1994, pp. 474–485.

[50] K. B. Khan, A. A. Khaliq, and M. Shahid, "A novel fast GLM approach for retinal vascular segmentation and denoising," *J. Inf. Sci. Eng.*, vol. 33, no. 6, pp. 1611–1627, 2017.

[51] A. Agresti and M. Kateri, "Categorical data analysis," in *International Encyclopedia of Statistical Science*, M. Lovric, Ed. Berlin, Germany: Springer, 2011.

[52] P. Coupé, P. Hellier, C. Kervrann, and C. Barillot, "Bayesian non local means-based speckle filtering," in *Proc. 5th IEEE Int. Symp. Biomed. Imag., Nano Macro*, May 2008, pp. 1291–1294.

[53] Y. Sato, S. Nakajima, H. Atsumi, T. Koller, G. Gerig, S. Yoshida, and R. Kikinis, "3D multi-scale line filter for segmentation and visualization of curvilinear structures in medical images," in *Proc. CVRMed-MRCAS*. Berlin, Germany: Springer, 1997, pp. 213–222.

[54] C. Lorenz, I.-C. Carlsen, T. M. Buzug, C. Fassnacht, and J. Weese, "Multi-scale line segmentation with automatic estimation of width, contrast and tangential direction in 2D and 3D medical images," in *Proc. CVRMed-MRCAS*. Berlin, Germany: Springer, 1997, pp. 233–242.

[55] T. H. J. M. Peeters, P. R. Rodrigues, A. Vilanova, and B. ter Haar Romeny, "Analysis of distance/similarity measures for diffusion tensor imaging," in *Visualization and Processing of Tensor Fields*. Berlin, Germany: Springer, 2009.

[56] T. Jerman, F. Pernuš, B. Likar, and V. Z. Špiclin, "Beyond Frangi: An improved multiscale vesselness filter," *Proc. SPIE*, vol. 9413, Mar. 2015, Art. no. 94132A.

[57] T. W. Ridler and S. Calvard, "Picture thresholding using an iterative selection method," *IEEE Trans. Syst., Man, Cybern.*, vol. SMC-8, no. 8, pp. 630–632, Aug. 1978.

[58] M. M. Fraz, P. Remagnino, A. Hoppe, B. Uyyanonvara, A. R. Rudnicka, C. G. Owen, and S. A. Barman, "An ensemble classification-based approach applied to retinal blood vessel segmentation," *IEEE Trans. Biomed. Eng.*, vol. 59, no. 9, pp. 2538–2548, Sep. 2012.

[59] E. Cheng, L. Du, Y. Wu, Y. J. Zhu, V. Megalooikonomou, and H. Ling, "Discriminative vessel segmentation in retinal images by fusing context-aware hybrid features," *Mach. Vis. Appl.*, vol. 25, no. 7, pp. 1779–1792, 2014.

[60] Q. Li, B. Feng, L. Xie, P. Liang, H. Zhang, and T. Wang, "A cross-modality learning approach for vessel segmentation in retinal images," *IEEE Trans. Med. Imag.*, vol. 35, no. 1, pp. 109–118, Jan. 2016.

[61] J. I. Orlando, E. Prokofyeva, and M. B. Blaschko, "A discriminatively trained fully connected conditional random field model for blood vessel segmentation in fundus images," *IEEE Trans. Biomed. Eng.*, vol. 64, no. 1, pp. 16–27, Jan. 2017.

[62] A. Dasgupta and S. Singh, "A fully convolutional neural network based structured prediction approach towards the retinal vessel segmentation," in *Proc. IEEE 14th Int. Symp. Biomed. Imag. (ISBI)*, Apr. 2017, pp. 248–251.

[63] Z. Yan, X. Yang, and K.-T. Cheng, "Joint segment-level and pixel-wise losses for deep learning based retinal vessel segmentation," *IEEE Trans. Biomed. Eng.*, vol. 65, no. 9, pp. 1912–1923, Sep. 2018.

[64] B. Zhanga, L. Zhangb, L. Zhangb, and F. Karraya, "Retinal vessel extraction by matched filter with first-order derivative of Gaussian," *Comput. Biol. Med.*, vol. 40, no. 4, pp. 438–445, Apr. 2010. [Online]. Available: http://www.sciencedirect.com/science/article/pii/S0010482510000302

[65] B. S. Y. Lam, Y. Gao, and A. W.-C. Liew, "General retinal vessel segmentation using regularization-based multiconcavity modeling," *IEEE Trans. Med. Imag.*, vol. 29, no. 7, pp. 1369–1381, Jul. 2010.

[66] M. S. Miri and A. Mahloojifar, "Retinal image analysis using curvelet transform and multistructure elements morphology by reconstruction," *IEEE Trans. Biomed. Eng.*, vol. 58, no. 5, pp. 1183–1192, May 2011.

[67] M. M. Fraz, S. A. Barman, P. Remagnino, A. Hoppe, A. Basit, B. Uyyanonvara, A. R. Rudnicka, and C. G. Owen, "An approach to localize the retinal blood vessels using bit planes and centerline detection," *Comput. Methods Programs Biomed.*, vol. 108, no. 2, pp. 600–616, 2012. [Online]. Available: http://www.sciencedirect.com/science/article/pii/S0169260711002276

[68] X. You, Q. Peng, Y. Yuan, Y.-M. Cheung, and J. Lei, "Segmentation of retinal blood vessels using the radial projection and semi-supervised approach," *Pattern Recognit.*, vol. 44, nos. 10–11, pp. 2314–2324, 2011. [Online]. Available: http://www.sciencedirect.com/science/article/pii/S0031320311000161

[69] G. Azzopardi, N. Strisciuglio, M. Vento, and N. Petkov, "Trainable COSFIRE filters for vessel delineation with application to retinal images," *Med. Image Anal.*, vol. 19, no. 1, pp. 46–57, Jan. 2015.
[70] B. Yin, H. Li, B. Sheng, X. Hou, Y. Chen, W. Wu, P. Li, R. Shen, Y. Bao, and W. Jia, "Vessel extraction from non-fluorescein fundus images using orientation-aware detector," *Med. Image Anal.*, vol. 26, no. 1, pp. 232–242, 2015. [Online]. Available: http://www.sciencedirect.com/science/article/pii/S1361841515001395
[71] J. Zhang, B. Dashtbozorg, E. Bekkers, J. P. W. Pluim, R. Duits, and B. M. T. H. Romeny, "Robust retinal vessel segmentation via locally adaptive derivative frames in orientation scores," *IEEE Trans. Med. Imag.*, vol. 35, no. 12, pp. 2631–2644, Dec. 2016.
[72] L. C. Neto, G. L. B. Ramalho, J. F. S. R. Neto, R. M. S. Veras, and F. N. S. Medeiros, "An unsupervised coarse-to-fine algorithm for blood vessel segmentation in fundus images," *Expert Syst. Appl.*, vol. 78, pp. 182–192, Jul. 2017.
[73] T. A. Soomro, J. Gao, Z. Lihong, A. J. Afifi, S. Soomro, and M. Paul, "Retinal blood vessels extraction of challenging images," in *Proc. Australas. Conf. Data Mining*. Singapore: Springer, 2018, pp. 347–359.
[74] Y. Zhao, Y. Liu, X. Wu, S. P. Harding, and Y. Zheng, "Retinal vessel segmentation: An efficient graph cut approach with retinex and local phase," *PLoS ONE*, vol. 10, no. 4, 2015, Art. no. e0122332.

AHSAN KHAWAJA was born in Abbottabad, Pakistan. He received the B.S. degree in computer system engineering from Comsats Abbottabad and the M.S. degree in micro-electronics and telecom from the University of Liverpool, U.K., in 2010. He is currently pursuing the Ph.D. degree in electrical engineering from Comsats University, Islamabad, Pakistan. His research interests include image enhancement and segmentation, pattern recognition, and color processing.

TARIQ M. KHAN received the B.S. degree in computer engineering from the COMSATS Institute of Information Technology, Islamabad, Pakistan, the M.Sc. degree in computer engineering from the University of Engineering and Technology, Taxila, Pakistan, and the Ph.D. degree in electronic engineering from Macquarie University Sydney, Australia, in 2016. He is currently working as an Assistant Professor with the Department of Electrical Engineering, COMSATS University Islamabad, Pakistan. He is interested in both digital image processing (with an emphasis on biometrics) and VLSI. His research interests include most aspects of image enhancement, pattern recognition, and image analysis. One area of particular interest is the application of FPGAs to implementing image processing algorithms.

KHURAM NAVEED received the M.S. degree in electrical engineering from COMSATS University Islamabad (CUI), Islamabad, Pakistan, in 2013. He is currently pursuing the Ph.D. degree with the Department of Electrical and Computer Engineering (ECE), CUI Islamabad, where he is also working as a Lecturer. His research interests include multiscale signal and image processing, multicomponent signal decomposition, and multivariate signal processing methods.

SYED SAUD NAQVI received the B.Sc. degree in computer engineering from the COMSATS Institute of Information Technology, Islamabad, Pakistan, and the M.Sc. degree in electronic engineering from the University of Sheffield, U.K., in 2005 and 2007, respectively, and the Ph.D. degree from the School of Engineering and Computer Science, Victoria University of Wellington, New Zealand, in 2016. He is currently working as an Assistant Professor with the COMSATS Institute of Information Technology. His research interests include saliency modeling, medical image analysis, scene understanding, and deep learning methods for image analysis.

NAVEED UR REHMAN received the Ph.D. degree in electrical engineering from the Imperial College London, U.K., in 2011. He is currently working as an Assistant Professor with the Department of Electrical and Computer Engineering, COMSATS University Islamabad, Pakistan. His research interests include multicomponent signal decomposition, time-frequency (T-F) analysis of non-stationary signals, multivariate or multichannel signal processing, and multiscale image processing methods.

SYED JUNAID NAWAZ (S'08–M'12–SM'16) received the Ph.D. degree in electronic engineering from Mohammad Ali Jinnah University, Islamabad, in February 2012. Since September 2005, he has been worked on various research and teaching positions with COMSATS University Islamabad (CUI), Islamabad, Pakistan, Staffordshire University, U.K., Federal Urdu University, Pakistan, The University of York, U.K., and the Aristotle University of Thessaloniki, Greece. He is currently working as an Assistant Professor with the Department of Electrical Engineering, CUI. His current research interests include signal processing, adaptive signal processing, compressed sensing, machine learning, wireless channel modeling and characterization, channel estimation and equalization, massive MIMO systems, mmWave channels, and vehicle-to-vehicle communications.